Condensate and final-state effects in superfluid ^{4}He

R. T. Azuah* and W. G. Stirling†
Department of Physics, University of Keele, Keele ST5 5BG, United Kingdom

H. R. Glyde and M. Boninsegni‡
Department of Physics and Astronomy, University of Delaware, Newark, Delaware 19716

P. E. Sokol
Department of Physics, Pennsylvania State University, University Park, Pennsylvania 16802

S. M. Bennington
ISIS Division, Rutherford Appleton Laboratory, Didcot OX11 0QX, United Kingdom
(Received 15 April 1997; revised manuscript received 11 August 1997)

We present high-precision measurements of the dynamics of single atoms in superfluid ^{4}He at $T=1.6$ K and saturated vapor pressure. The measurements were taken on the MARI instrument at the ISIS neutron-scattering facility, Rutherford-Appleton Laboratory. From the measurements we obtain a condensate fraction $n_0=6.0\pm2.0\%$ at $T=1.6$ K. The final-state effects (FSE's) in the atomic response are also determined from the data in the form of a final-state broadening function, $R(Q,y)$. We find that this FS function is the same in the superfluid at $T=1.6$ K as that determined previously in normal ^{4}He at $T=2.3$ K. If we reanalyze the data assuming that the superfluid has no condensate, i.e., $n_0=0$, then the data requires that the normal $n(\mathbf{k})$ change dramatically between $T=2.3$ K and $T=1.6$ K. Since such a change in $n(\mathbf{k})$ is physically unexpected, given that kT is much less than the zero-point energy, the data requires that a new contribution, such as a condensate, enter $n(\mathbf{k})$ in the superfluid. [S0163-1829(97)04946-1]

I. INTRODUCTION

Bose-Einstein condensation plays a special role in quantum physics. Bose[1] and Einstein[2] proposed that a gas of noninteracting bosons would condense into a state characterized by macroscopic occupation of one single-particle quantum state. London[3] suggested that this condensation is the origin of superfluidity in liquid ^{4}He at temperatures below $T_\lambda=2.17$ K. Superconductivity in a wide spectrum of materials is now identified with condensation of paired fermions (composite bosons).[4] Spectacular bose condensation in which nearly the entire system is condensed into a single atomic state has recently been observed in trapped, dilute gases of alkali atoms.[5,6]

Liquid ^{4}He remains the most accessible pure bose liquid in nature and a key model system.[7–9] Because of the strong interaction between the ^{4}He atoms in the liquid, particularly the repulsive core, the fraction n_0 of atoms that condense into the zero-momentum ($\mathbf{k}=0$) state is small, approximately 10% at $T=0$.[10–16] The clear verification that there is indeed a condensate and the accurate determination of n_0 remain an important goal. Taking advantage of significant improvements in neutron source intensity and instrumentation, we present accurate data and analysis methods which we believe show unambiguously that superfluid ^{4}He has a condensate, with a condensate fraction $n_0=6.0\pm2.0\%$ at $T=1.6$ K.

Miller *et al.*[17] and Hohenberg and Platzman[18] proposed that the condensate fraction n_0 could be observed in the dynamic structure factor $S(Q,\omega)$ of superfluid ^{4}He. Essentially, in neutron-scattering measurements of $S(Q,\omega)$ at high wave vector (Q) transfer, the energy transfer ω is Doppler broadened by the momentum distribution, $n(\mathbf{k})$, of the atoms in the fluid. When there is a condensate, the fraction $n_0=n(\mathbf{k}=0)$ of atoms in the condensate contributes an ''unbroadened'' peak to $S(Q,\omega)$. This peak appears in $S(Q,\omega)$ at $\omega=\omega_R$ where $\omega_R=\hbar Q^2/2M$ is the free, stationary, atom recoil frequency and M is the atomic mass. Expressed in the y-scaling variable, $y=(\omega-\omega_R)/(\hbar Q/M)$, the peak appears at $y=0$. The atoms struck by the neutrons recoil in the fluid. If their interaction with their neighbors is neglected, denoted the impulse approximation (IA), n_0 can be extracted directly from $S(Q,\omega)$.

Early measurements of n_0 using neutrons (up to 1976) are summarized by Martel *et al.*[19]. These measurements yielded a wide range of n_0 values. This is because the interactions of recoiling atoms with their neighbors in the fluid, denoted final-state effects (FSE's), are not negligible, but rather contribute significantly to the observed $S(Q,\omega)$. Gersch and Rodriguez[20] presented a systematic discussion of FSE's in $S(Q,\omega)$. In their formulation, FSE's are accounted for via a broadening function $R(Q,y)$, to be convoluted with the IA to obtain $S(Q,\omega)$.

Sears[21] developed a formulation in which FSE's appear as additive corrections to the IA. Based on this formulation, and using neutron-scattering data in the range $Q\sim10$ Å^{-1}, Sears *et al.*[10] obtained values of $n_0\approx13.9\pm2.3\%$ and $n_0\approx10.9\pm2.7\%$ at $T=0$ and saturated vapor pressure (SVP).

Sokol and collaborators[12–16] made an extensive series of pioneering measurements at higher Q values ($Q\simeq20$–30 Å^{-1}), using the first spallation neutron source IPNS at Argonne National Laboratory. From these measurements a con-

densate fraction $n_0=10\pm2\%$ at $T=0$ and SVP was determined, as well as the temperature and pressure dependence of n_0. In this case, the convolution approach of Gersch and Rodriguez and the FSE function $R(Q,y)$ calculated by Silver[23] were used to account for final-state contributions.

Taking advantage of the increased beam intensity at ISIS and the improved instrumental resolution of MARI, we have recently presented precision measurements of the dynamic structure factor $S(Q,\omega)$ of normal ^{4}He at $T=2.3$ K and at SVP. From the data, both $n(\mathbf{k})$ and the Final State broadening function $R(Q,y)$ in normal ^{4}He were accurately determined.[22] The momentum distribution $n(\mathbf{k})$ in normal ^{4}He at SVP differs significantly from a Gaussian, with large occupation of the low-lying $\mathbf{k}$ states. The extracted $n(\mathbf{k})$ agrees well with theoretical calculations. These calculations[24] also show that $n(\mathbf{k})$ for $\mathbf{k}>0$ changes little with temperature, as might be expected for a cold quantum liquid in which the zero-point kinetic energy ($\sim$ 15 K) dominates the thermal energy ($\sim$ 2 K). The $R(Q,y)$ is similar in shape to those calculated by Silver[25] and by Carraro and Koonin,[26] but is less peaked and broader than the calculated $R(Q,y)$'s.

The aim of this paper is to determine both n_0 and $R(Q,y)$ accurately in superfluid ^{4}He ($T\leqslant T_\lambda$). We have made precision measurements of $S(Q,\omega)$ in the wave-vector range $15\leqslant Q\leqslant 29$ Å^{-1}, in which FSE are not negligible. The data are presented as $J(Q,y)=(\hbar Q/M)S(Q,\omega)$ where y is the scaling variable and analyzed using a method developed by Glyde.[27] Assuming that $n^\star(\mathbf{k})$, the momentum distribution of the $\mathbf{k}>0$ states above the condensate has the same shape as $n(\mathbf{k})$ in the normal ^{4}He at $T=2.3$ K, we determine n_0 and $R(Q,y)$ in the superfluid at $T=1.6$ K. We obtain $n_0=6.0\pm2.0\%$ and an $R(Q,y)$ that is the same as in the normal phase. In a second analysis of the data, we assume that there is no condensate ($n_0=0$) and that $R(Q,y)$ is the same at $T=1.6$ and 2.3 K, and determine a ''normal'' $n(\mathbf{k})$ at $T=1.6$ K. We show that this normal $n(\mathbf{k})$ is unphysical and interpret this as definitive evidence that there is a condensate in superfluid ^{4}He at SVP below T_λ.

In Secs. II and III, we discuss the method of analyzing the data and the experimental details, respectively. The results are presented in Sec. IV where we particularly test the sensitivity of the results to variation of analysis assumptions. The results are discussed in Sec. V.

II. THEORETICAL BACKGROUND

At high momentum transfer ($Q\geqslant 10$ Å^{-1} in helium), the incoming neutron scatters from a single atom. In this limit, the observed dynamic structure factor, $S(Q,\omega)$, is well approximated by the incoherent structure factor[9]

$$S_i(Q,\omega)=\int dt e^{i\omega t}S_i(Q,t), \tag{1}$$

where the intermediate scattering function,

$$S_i(Q,t)=\langle e^{-i\mathbf{Q}\cdot\mathbf{r}(t)}e^{i\mathbf{Q}\cdot\mathbf{r}(0)}\rangle = e^{-i\omega_R t}\langle T_t e^{-i(\hbar Q/M)\int_0^t dt' k_Q(t')}\rangle, \tag{2}$$

describes the motion of a single atom in the fluid. Here r is the position of the atom struck by the neutron, $\hbar\omega_R=(\hbar Q)^2/(2M)$ and $v_R=\hbar Q/M$ are, respectively, the free atom recoil energy and velocity, and $\hbar k_Q=\hbar\mathbf{k}\cdot\mathbf{Q}/Q$ is the momentum of the struck atom along $\mathbf{Q}$; $\langle\ldots\rangle$ indicates a thermal average. The second expression is useful at short scattering times, t, (high Q and ω), and T_t is the time ordering operator.

At high Q, $S_i(Q,\omega)$ and $S_i(Q,t)$ are approximately independent of Q if expressed in terms of the wave-vector variable $y=(\omega-\omega_R)/(\hbar Q/M)$ and its conjugate variable $s=(\hbar Q/M)t$, respectively. The approximately Q-independent forms are $J(Q,y)=(\hbar Q/M)S(Q,\omega)$ and

$$J(Q,s)\equiv e^{i\omega_R t}S_i(Q,t)=\langle T_s e^{-i\int_0^s ds' k_Q(s')}\rangle \tag{3}$$

with

$$J(Q,y)=\int ds\ e^{iys}J(Q,s). \tag{4}$$

We present all data in the form $J(Q,y)$ in this paper. In Eq. (3), $k_Q(s)$ is the wave vector of the struck atom after it has traveled a distance $s=(\hbar Q/M)t$ from the scattering event. At high Q, the struck atom travels a short distance s in the fluid. In the IA we assume s is so short that $k_Q(s)$ at all s can be approximated by $k_Q(0)$ at $s=0$. This means that all collisions with neighbors in the final-state which change k_Q are ignored. In this case $J(Q,s)$ in Eq. (3) reduces to

$$J_{\mathrm{IA}}(s)=\langle e^{-ik_Q s}\rangle. \tag{5}$$

The one-body density matrix (OBDM), i.e., the Fourier transform of the momentum distribution $n(\mathbf{k})$, is

$$n(\mathbf{r})=\frac{1}{n}\langle\Psi^+(0)\Psi(r)\rangle=\langle e^{-i\mathbf{k}\cdot\mathbf{r}}\rangle. \tag{6}$$

Comparing Eqs. (5) and (6), we see that $J_{\mathrm{IA}}(s)$ is the OBDM for displacements of $\mathbf{r}$ along $\mathbf{Q}$, $\mathbf{k}\cdot\mathbf{r}=k_Q s$, i.e.,

$$J_{\mathrm{IA}}(s)=n(s)=n(\mathbf{r}\cdot\hat{\mathbf{Q}}). \tag{7}$$

For a spherically symmetric fluid, $n(s)$ and $n(\mathbf{r})$ are the same function. The Fourier transform of $n(s)$,

$$J_{\mathrm{IA}}(y)=n(y)=\int ds\ e^{iys}J_{\mathrm{IA}}(s), \tag{8}$$

is the longitudinal momentum distribution $n(y)=\int dk_x dk_y n(k_x,k_y,k_Q)$ for momentum variable $y=k_Q=\mathbf{k}\cdot\hat{\mathbf{Q}}$ along Q.

When final-state interactions are important, the intermediate function $J(Q,s)$ can be formally expressed in terms of $J_{\mathrm{IA}}(s)$ as

$$J(Q,s)=J_{\mathrm{IA}}(s)R(Q,s), \tag{9}$$

which defines the final-state function $R(Q,s)$. From Eq. (4), the observed scattering function is

$$J(Q,y)=\int ds\ e^{iys}J_{\mathrm{IA}}(s)R(Q,s). \tag{10}$$

In the following section, we introduce a model for $n(\mathbf{k})$. This consists of a condensate component plus a ''noncondensate'' component arising from the states with $\mathbf{k}\neq 0$. The $n(\mathbf{k})$ is Fourier transformed to obtain $n(s)=J_{\mathrm{IA}}(s)$. As noted, at high Q the scattering time and s are short. For $R(Q,s)$, we use an expansion in powers of s up to s^6. $J(Q,y)$ is then obtained from Eq. (10) and fitted to experiment to obtain n_0 and the coefficients in the expansion of $R(Q,s)$.

Model of $n(\mathbf{k})$

When there is a condensate we have a macroscopic occupation of the $\mathbf{k}=0$ state and large occupation of states with very low $\mathbf{k}$. This leads to long-range components in $J_{\mathrm{IA}}(s)=n(s)$. To describe $n(\mathbf{k})$, we introduce the following model:

$$n(\mathbf{k})=n_0[\,\delta(\mathbf{k})+f(\mathbf{k})\,]+A_1 n^{\star}(\mathbf{k}). \tag{11}$$

Here $n_0\delta(\mathbf{k})$ is the condensate contribution and

$$n_0 f(\mathbf{k})=\frac{n_0 Mc}{2\hbar(2\pi)^3 n}\,\frac{1}{|\mathbf{k}|}\,\coth\!\left(\frac{c\hbar|\mathbf{k}|}{2k_B T}\right)e^{-\mathbf{k}^2/(2k_c^2)} \tag{12}$$

describes the high occupation of low momentum states resulting from the excitation of quasiparticles out of the condensate and the coupling between these quasiparticles and phonons in the range $0\leqslant\mathbf{k}\leqslant 0.7\ \text{Å}^{-1}$. The first two terms in Eq. (11) are clearly terms in $n(\mathbf{k})$ arising from the condensate and are proportional to n_0. In the expression for $f(\mathbf{k})$, c is the speed of sound in liquid helium and $n=N/V$ is the liquid density. The functional form of $f(\mathbf{k})$ can be derived directly[8,9,28] at low $\mathbf{k}$ and is given by the terms in Eq. (12) except for the Gaussian. We have multiplied the known terms by a Gaussian in order to cut off $f(\mathbf{k})$ at higher $\mathbf{k}$ since $f(\mathbf{k})$ must terminate at the end of the phonon region at $\mathbf{k}\simeq 0.7\ \text{Å}^{-1}$. We have set $k_c=0.5\ \text{Å}^{-1}$, which is a parameter in the model. We will test the sensitivity of n_0 to k_c.

The term $A_1 n^{\star}(\mathbf{k})$ describes the momentum distribution for the $\mathbf{k}>0$ states above the condensate uncoupled to it. A central assumption made here is that this $n^{\star}(\mathbf{k})$ has the same functional form as $n(\mathbf{k})$ in normal ^{4}He. For $n^{\star}(\mathbf{k})$ we use the accurately determined[22] momentum distribution of normal ^{4}He at $T=2.3$ K. This $n^{\star}(\mathbf{k})$ is conveniently expressed as the Fourier transform of $n(s)$, given by

$$n^{\star}(s)=\exp\!\left[-\frac{\overline{\alpha_2}s^2}{2!}+\frac{\overline{\alpha_4}s^4}{4!}-\frac{\overline{\alpha_6}s^6}{6!}\right] \tag{13}$$

with $\overline{\alpha_2}=0.897\ \text{Å}^{-2}$, $\overline{\alpha_4}=0.46\ \text{Å}^{-4}$ and $\overline{\alpha_6}=0.38\ \text{Å}^{-6}$. This expression for $n^{\star}(s)$ is correct up to terms s^6 for a normal fluid (see Appendix A) and

$$\overline{\alpha_2}=\langle k_Q^2\rangle, \tag{14}$$

$$\overline{\alpha_4}=\langle k_Q^4\rangle-3\langle k_Q^2\rangle^2,$$

$$\overline{\alpha_6}=\langle k_Q^6\rangle-15\langle k_Q^4\rangle\langle k_Q^2\rangle+30\langle k_Q^2\rangle^3$$

are cumulants of $n(k_Q)$. The calculations of Ceperley and Pollock[24] show that $n^{\star}(\mathbf{k})$ does not change with temperature between 1.18 and 2.5 K within calculational error which we discuss further below.

The two parameters in the model $n(\mathbf{k})$ are n_0 and k_c, with A_1 determined so that $n(\mathbf{k})$ is normalized, which typically gives $A_1\approx 0.91$. For $k_c=0.5\ \text{Å}^{-1}$, $\int d\mathbf{k}\, f(\mathbf{k})\simeq 0.5$ and the $n_0 f(\mathbf{k})$ term contributes 30% of the condensate induced weight in Eq. (11). This defines the model $n(\mathbf{k})$. We Fourier transform this $n(\mathbf{k})$ to obtain $n(s)$ in the form

$$J_{\mathrm{IA}}(s)=n(s)=n_0[1+f(s)]+A_1 n^{\star}(s). \tag{15}$$

For the final-state function $R(Q,s)$ we use an expansion in powers of s that can be obtained directly from its definition in Eq. (9) (see Appendix A). Up to powers s^6, this is

$$R(Q,s)=\exp\!\left[\frac{i\overline{\beta_3}s^3}{3!}+\frac{\overline{\beta_4}s^4}{4!}-\frac{i\overline{\beta_5}s^5}{5!}-\frac{\overline{\beta_6}s^6}{6!}+\cdots\right]. \tag{16}$$

The coefficients $\overline{\beta_n}$ are given by

$$\overline{\beta_3}=\overline{a_3}/\lambda Q, \tag{17}$$

$$\overline{\beta_4}=\overline{a_4}/(\lambda Q)^2,$$

$$\overline{\beta_5}=\overline{a_{52}}/(\lambda Q)^3+\overline{a_{54}}/\lambda Q,$$

$$\overline{\beta_6}=\overline{a_{62}}/(\lambda Q)^4+\overline{a_{64}}/(\lambda Q)^2.$$

In Eq. (17), the $\overline{a_n}$ are independent of Q and $\lambda=\hbar^2/M=1.0443$ meV Å^2. The $\overline{\beta_n}$ clearly decrease with increasing Q and, for $Q\to\infty$, $R(Q,s)\to 1$, i.e., the IA. Analytic expressions for the $\overline{a_n}$ can be derived.[21,27] For example, $\overline{a_3}=\langle\nabla^2 V(r)\rangle/6$ and $\overline{a_4}=\langle\mathbf{F}\cdot\mathbf{F}\rangle/3$ where $\mathbf{F}=-\nabla V(r)$ is the force on an atom. The series (16) was derived strictly using the relation $J(Q,s)=n^{\star}(s)R(Q,s)$ and the central role of $R(Q,s)$ is to cut off $J(Q,s)$ at large s. In the presence of a condensate, we have added a constant term to $n^{\star}(s)$ in Eqs. (15) and (9) [$f(s)$ is long range in s] and we do not expect the added constant to change the nature of the cut off significantly (see Appendix A).

In summary, $J(Q,y)$ is given by Eq. (10) with $J_{\mathrm{IA}}(s)=n(s)$ given by Eq. (15) and $R(Q,s)$ given by Eq. (16). The $J(Q,y)$ is fitted to experiment to determine n_0, and the parameters $\overline{\beta_3}$, $\overline{\beta_4}$, $\overline{\beta_5}$, and $\overline{\beta_6}$ in $R(Q,s)$.

III. DATA COLLECTION AND REDUCTION

The measurements were carried out at the ISIS pulsed spallation neutron source at the Rutherford Appleton Laboratory in the United Kingdom. The instrument used was the high-energy direct geometry chopper spectrometer MARI with incident energies up to 1000 meV possible. More than 650 ^{3}He gas detectors provide an almost continuous coverage of scattering angles, ϕ, between 3° and 135° in steps of 0.43°. This makes it possible to measure a large range in momentum and energy transfer in a single experiment scan. Due to the pulsed nature of the source, data collection is performed in time-of-flight (TOF) in which the time of arrival of a neutron in the detector, measured from when they leave the moderator, determines its energy loss or gain after scattering from the sample. The momentum transfer depends on the TOF and the scattering angle of the neutron. A high-

purity sample of ^{4}He gas was condensed into a cylindrical aluminium can of length 5 cm and diameter 5 cm placed inside a standard ^{4}He ''orange'' cryostat. To minimize multiple scattering of neutrons within the sample, the cylindrical sample volume was split into eight smaller cylindrical sections using highly neutron absorbing boron nitride disks. The sample temperature was maintained at 1.6 ± 0.05 K using a Lakeshore temperature controller and a Germanium diode sensor. As an independent check, the resistance thermometry readings were compared to the vapor pressure readings of the sample. The measurement was made at saturated vapor pressure. In order to cover the (Q,ω) range of interest, an incident neutron energy of 755 meV was employed. A measurement was also made with the sample cell empty to determine the sample independent background scattering.

The collected data in TOF was then converted to energy transfer $(\hbar\omega)$ at constant scattering angle using standard procedures. The reader is referred to the recent article by Andersen *et al.*[29] for a detailed discussion of the data transformation from TOF to $S(\phi,\omega)$ and then to $S(Q,\omega)$. In this article we have made use of the inherent scaling property of the scattering function with Q in the IA generally known as y scaling and referred to in the last section. In the IA, the scattering function can be portrayed as the longitudinal momentum distribution $J_{\rm IA}(y)$ where $y=(\omega-\omega_R)(M/\hbar Q)$ and $J_{\rm IA}(y)=(\hbar Q/M)S_{\rm IA}(Q,\omega)$, and does not depend on Q and ω separately. However, at moderate Q where the IA does not apply, y scaling is still approximately observed and it is useful to present the data as a generalized longitudinal momentum distribution $J(Q,y)=(\hbar Q/M)S(Q,\omega)$ as in Eq. (4) which is weakly Q dependent as a result of FSE's. The experimental data were transformed to $J(Q,y)$ for $Q=15$ to 29 Å^{-1} in steps of 0.5 Å^{-1} and a sample of the data are shown in Fig. 1. The statistical accuracy of the data is very high.

The observed $J(Q,y)$ consists of a convolution of the underlying momentum distribution, the FS function and the instrumental resolution function. Hence, for a quantitative analysis of the data, the instrumental resolution function must be accurately known. We have used a Monte Carlo simulation method to calculate the instrumental resolution.[30] In this method, the neutron-scattering experiment is simulated using the known instrument parameters, sample cell geometry and an estimate for the sample scattering function. The incident neutron beam characteristics were modeled using the Ikeda-Carpenter[31] speed and time distribution function with the adjustable parameters determined from a fit to the experimental monitor peaks before and after the sample. The simulation results are obtained in TOF and are then treated in the same way as the experimental data. The result is a convolution between the instrumental resolution function, $I(Q,y)$, and the model scattering function input to the simulation. $I(Q,y)$ is then simply deconvoluted from the simulation. The resulting instrumental resolution function is shown as a dashed line in Fig. 1. It is seen that $I(Q,y)$ narrows with increasing Q and is very small at large Q thus increasing the reliability of the data.

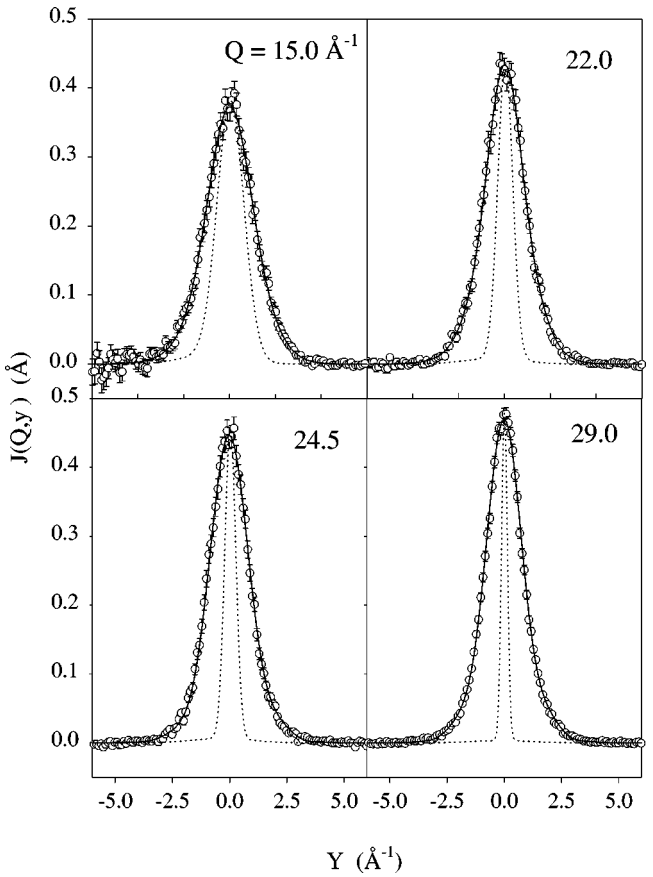

FIG. 1. Observed scattering intensity expressed as $J(Q,y)$ at constant $Q=15$, 22, 24.5, and 29 Å^{-1}, in superfluid ^{4}He at $T=1.6$ K and saturated vapor pressure. The dotted lines are the calculated instrumental resolution function and the solid lines are fits to the data using the model $J(Q,y)$ function described in the text.

IV. RESULTS

A. Fitted n_0 and $R(Q,y)$

Figure 1 shows the observed data at four Q values between $Q=15$ Å^{-1} and $Q=29$ Å^{-1}. The solid line is the fit of $J(Q,y)$ given by Eq. (10) using the model momentum distribution in Eq. (15) and the final-state broadening function given by Eq. (16) to the data. The free parameters in the fit are n_0, $\overline{\beta_3}$, $\overline{\beta_4}$, $\overline{\beta_5}$, and $\overline{\beta_6}$. The cutoff parameter k_c in $f(\mathbf{k})$ was set at 0.5 Å^{-1} and the parameters $\overline{\alpha_2}$, $\overline{\alpha_4}$, $\overline{\alpha_6}$ in $n^\star(\mathbf{k})$ were set at the values determined[22] for normal ^{4}He, $\overline{\alpha_2}=0.897$ Å^{-2}, $\overline{\alpha_4}=0.46$ Å^{-4}, $\overline{\alpha_6}=0.38$ Å^{-6}. The dotted line in Fig. 1 is the instrumental resolution function (IRS). The fits to the data are clearly good both in the peak and the tail regions of the data. Fits as shown in Fig. 1 were made to data at 29 separate Q values between $Q=15$ Å^{-1} and $Q=29$ Å^{-1}. The fit procedure and errors in the parameters are discussed in Appendix B.

The values obtained for the fitted parameters are shown as functions of Q in Fig. 2. Figure 2(a) shows n_0. The n_0 is independent of Q with an average value of $n_0=5.0\pm1.5\%$ indicated by the solid line. The precision in determining n_0 increases with increasing Q because the IRS narrows with increasing Q. As noted in Eq. (17), $\overline{\beta_3}$ is expected to be $\overline{\beta_3}=\overline{a_3}/(\lambda Q)$ where $\overline{a_3}=\langle\nabla^2V(r)\rangle/6$ is independent of Q. Figure 2(b) shows $\overline{\beta_3}Q$ versus Q which indeed turns out to be independent of Q with $\overline{a_3}/\lambda=2.75\pm1.0$ Å^{-4}. In the fits we found $\overline{\beta_4}=0$ within the fitted error and we set $\overline{\beta_4}=0$. Again as noted in Eq. (17) $\overline{\beta_5}$ has two terms. Figure 2(c)

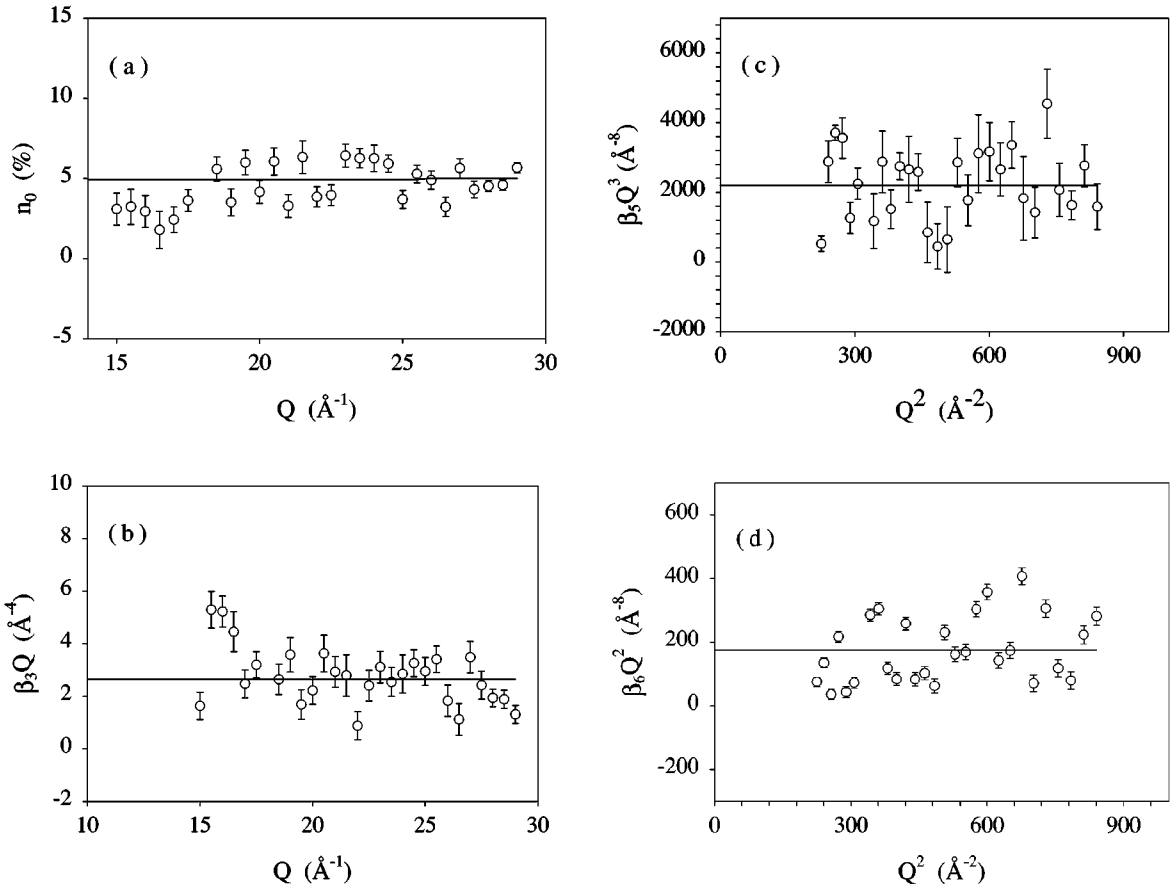

FIG. 2. Parameters obtained by fitting the model $J(Q,y)$ to superfluid ^{4}He data as shown in Fig. 1 as a function of the wave-vector transfer, Q. The fitted parameters are (a) the condensate fraction n_0, and the parameters for the final-state function (b) $\overline{\beta_3}$, (c) $\overline{\beta_5}$, and (d) $\overline{\beta_6}$.

shows the values of $\overline{\beta_5}$ obtained in the fits, plotted as $\overline{\beta_5}Q^3$ vs Q^2. This shows that $\overline{\beta_5}Q^3$ is independent of Q, within our precision. This means that the term $\overline{a_{52}}/\lambda Q^3$ in $\overline{\beta_5}$ dominates, and that $\overline{a_{54}}=0$ within precision. The Q-independent value of $\overline{\beta_5}Q^3$ gives $\overline{a_{52}}/\lambda^3=2200\pm800$ Å^{-8}.

Finally, Fig. 2(d) shows $\overline{\beta_6}Q^2$ which turns out to be independent of Q. This means that $\overline{a_{62}}=0$ within error and $\overline{a_{64}}/\lambda^2=175\pm75$ Å^{-8}. These values of $\overline{a_3}$, $\overline{a_{52}}$, and $\overline{a_{64}}$ determine the final-state broadening function in the form

$$R(Q,s)=\exp\left[\frac{is^3}{3!}\frac{\overline{a_3}}{\lambda Q}-\frac{is^5}{5!}\frac{\overline{a_{52}}}{(\lambda Q)^3}-\frac{s^6}{6!}\frac{\overline{a_{64}}}{(\lambda Q)^2}\right]. \quad (18)$$

Figure 3 compares the FS function, $R(Q,y)$, obtained here (solid line) with that obtained previously[22] in normal ^{4}He at $T=2.3$ K (dashed line). We see that the two $R(Q,y)$'s agree within determined precision. The main difference between the two is that the normal ^{4}He $R(Q,y)$ is peaked at a somewhat lower (more negative) y value. This reflects the larger mean value of $\overline{a_3}$ found in the normal ^{4}He ($\overline{a_3}/\lambda=3.3\pm0.7$ Å^{-4}). The two $\overline{a_3}$ values agree within the determined error of the fits. From this comparison, we find that $R(Q,y)$ is the same in the normal and superfluid phases of liquid ^{4}He.

B. Variation of parameters

In order to test the sensitivity to parameters in the fits, we show results with some preset parameters.

1. Dependence on n_0

Figures 4 and 5 show fits to data with n_0 set at $n_0=0$ and $R(Q,y)$ refitted to the data at $Q=19.5$ Å^{-1} and $Q=29$ Å^{-1},

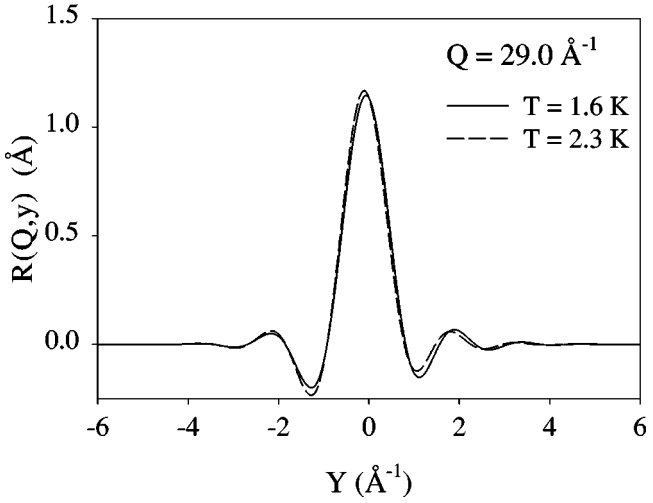

FIG. 3. The extracted final-state function at $Q=29$ Å^{-1} in superfluid ^{4}He at $T=1.6$ K (solid line) compared to that obtained previously (Ref. 22) in normal ^{4}He at $T=2.3$ K (dashed line).

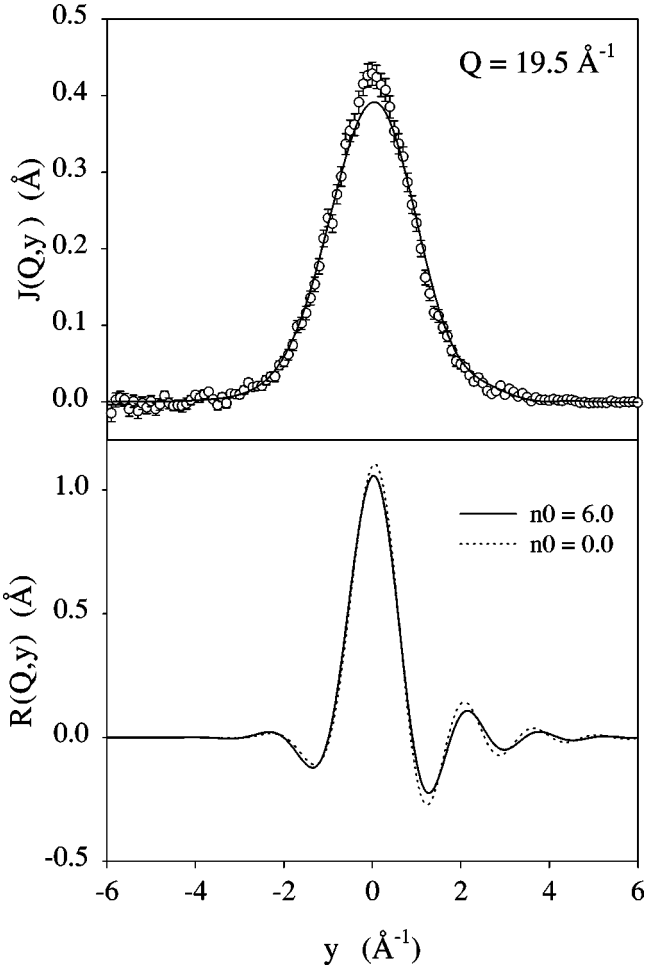

FIG. 4. Upper frame; Fit of the model scattering function to data at $Q=19.5$ Å^{-1} with n_0 fixed at 0%. Lower frame; the resulting $R(Q,y)$ for the fit (solid line) is compared with the best fit $R(Q,y)$ (dashed line) for the same Q in the lower frame of the figure.

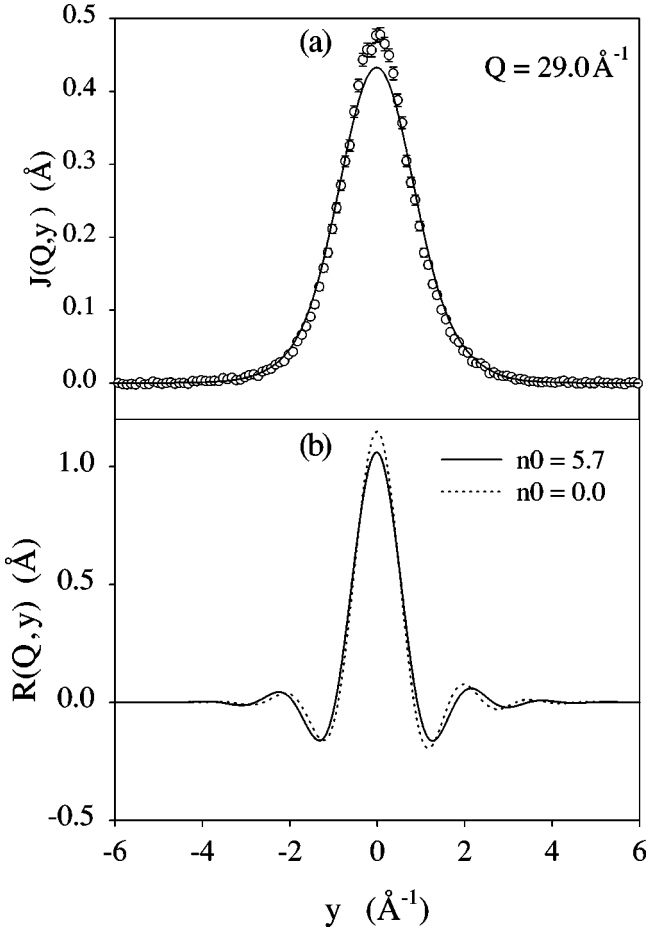

FIG. 5. Same as Fig. 4 for $Q=29$ Å^{-1}.

respectively. In this case, the normalization factor in Eq. (11) is $A_1=1.0$, which leads to a broader $n(\mathbf{k})$. Clearly the fit of $J(Q,y)$ in Figs. 4(a) and 5(a) is too low around $y=0$ where n_0 contributes the most. The fit is also broader than the data throughout most of $J(Q,y)$. Essentially, the fitted $R(Q,y)$ with $n_0=0$ [the dashed line in Figs. 4(b) and 5(b)] cannot become narrow enough to provide a good fit to the data. We believe this is because as $R(Q,y)$ becomes narrower, the amplitude of the oscillations in $R(Q,y)$ for $|y|\geqslant 1$ Å^{-1} becomes larger. These oscillations appear in $R(Q,y)$ because it is normalized to unity and its first and second moments equal zero. There is no evidence of oscillations in the data. Thus, a best fit in the wings and near $y=0$ leads to a $J(Q,y)$ that is broad, too low at $y=0$ and has modest oscillations. Essentially it is not possible to fit the data in superfluid ^{4}He using the $n(\mathbf{k})$ from normal ^{4}He and fitting $R(Q,y)$.

Figure 6 shows fits to data at $Q=29$ Å^{-1} with n_0 set at 0%, 5.7% (the best-fit value) and 10% with $R(Q,y)$ adjusted in each case to get the best fit. Clearly the $n_0=5.7\%$ is the best fit both in the wings and in the peak region. In the $n_0=10\%$ case the fit is too high in the peak and too low near $y=\pm 1.5$ Å^{-1}. For $n_0=10\%$, if $R(Q,y)$ were broadened further to fit the data in the peak region, it would be at the expense of a much poorer fit in the wings.

To test the sensitivity of n_0 to the cut off k_c, we fixed k_c at 0.3, 0.5 and 0.7 Å^{-1} and fitted for n_0 in each case and obtained 6.4, 5.7, and 5.4%, respectively, at $Q=29$ Å^{-1}. Essentially a lower value of k_c means a smaller contribution to $n(\mathbf{k})$ from $f(\mathbf{k})$ and a corresponding larger n_0 is required to fit the data. The quality of the fit to the data for the different k_c values is the same as shown in Fig. 1. Given the sensitivity to k_c and that the fits are low, rather than high, in the peak region of $J(Q,y)$, we take our observed n_0 value as $n_0=6\pm 2\%$. Reasonable lower and upper limits to k_c are 0.3 and 0.7 so that the additional error in n_0 arising from the uncertainty in k_c is $\pm 0.5\%$.

2. Dependence on $n^\star(\mathbf{k})$

We now assume that there is no condensate in superfluid ^{4}He and present fits to the data in which n_0 is set to zero and $n^\star(\mathbf{k})$ is adjusted to obtain a fit. For this fit, we set $R(Q,y)$ to that determined[22] in the normal phase at $T=2.3$ K. Since $R(Q,y)$ depends on interactions which change little with temperature, the $R(Q,y)$ from normal ^{4}He is a logical choice for $n_0=0$. The upper frame of Fig. 7 shows a fit to data at $Q=29$ Å^{-1}. It is seen that a good fit is possible. However, the $n(\mathbf{k})$ obtained is physically quite unrealistic. The lower frame of Fig. 7 shows this $n(\mathbf{k})$ as the dotted line. In the same frame, the solid line shows $n(\mathbf{k})$ observed[22] in normal ^{4}He at $T=2.3$ K; the points show $n(\mathbf{k})$ at three temperatures calculated by Ceperley and Pollock (CP)[24].

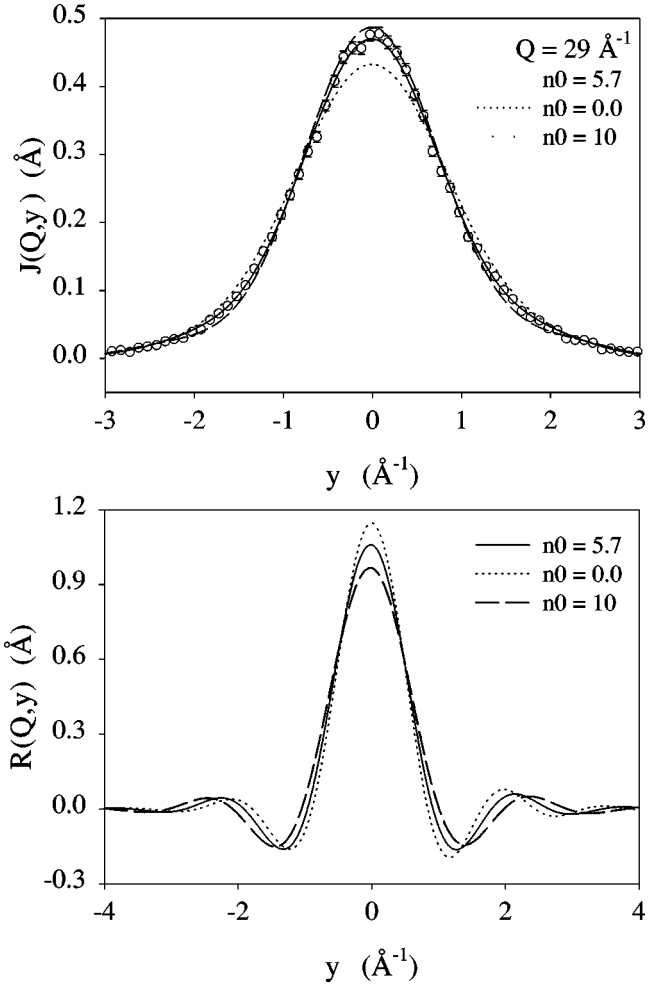

FIG. 6. Sensitivity of the model to n_0. When n_0 is too high (10%) or too low (0%), it is not possible to fit the data by adjusting $R(Q,y)$. The change in the fitted $R(Q,y)$ obtained for these extremes in n_0 are shown in the lower frame.

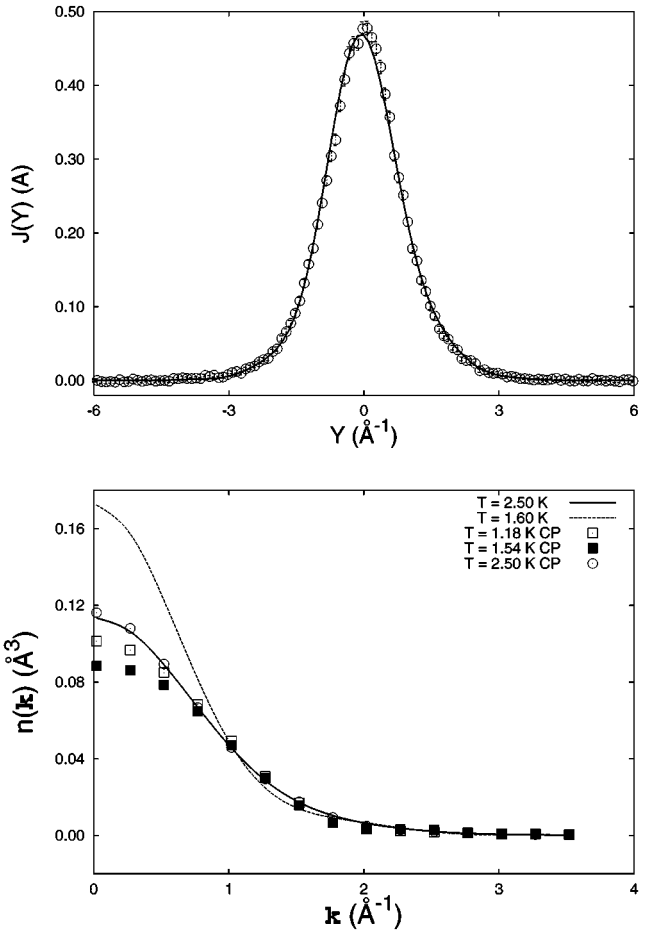

FIG. 7. Upper frame; Fit to data at $Q=29$ Å^{-1}, $T=1.6$ K and $n_0=0$ with $R(Q,y)$ fixed at the normal ^{4}He value (see Fig. 3) and $n(\mathbf{k})$ varied to obtain a fit. Lower frame shows the resulting $n(\mathbf{k})$ obtained from this fit (dotted line) compared with the $n(\mathbf{k})$ in normal ^{4}He at $T=2.3$ K (solid line). The CP are the PIMC calculations of $n(\mathbf{k})$ by Ceperley and Pollock (CP) at three temperatures. The CP $n(\mathbf{k})$ for $T<T_\lambda$ are normalized to slightly less than unity because of the condensate.

Clearly, the fit to $J(Q,y)$ with $n_0=0$ at $T=1.6$ K produces an $n(\mathbf{k})$ which differs markedly from the observed $n(\mathbf{k})$ at $T=2.3$ K and the calculated $n(\mathbf{k})$ at all three temperatures. Such a dramatic change in $n(\mathbf{k})$ when T is decreased from 2.3 to 1.6 K is phyically unexpected, given that $T=2.3$ K is already much less than the zero-point energy. That is, the kinetic energy per atom is $\sim$ 15 K which is much larger than the thermal energy $3T/2$. At $T=2.3$ K, liquid ^{4}He is already a ''cold'' quantum liquid and $n(\mathbf{k})$ differs markedly from a classical Gaussian distribution. On further cooling by $\Delta T=0.7$ K, we would not expect a significant, additional change in $n(\mathbf{k})$, were there no transition. Yet, a large change of $n(\mathbf{k})$ between $T=2.3$ K and $T=1.6$ K is required to fit the data, if no condensate is included. There would be no physical reason for such a change. In other words, a reasonable fit to the data with $n_0=0$ cannot be obtained.

V. DISCUSSION

A key assumption made here to obtain n_0 shown in Figs. 1 and 2 is that the momentum distribution $n^\star(\mathbf{k})$ over the $\mathbf{k}>0$ states uncoupled from n_0 is independent of temperature between 1.6 and 2.3 K. This allows us to use the accurately determined $n(\mathbf{k})$ in normal ^{4}He at T=2.3 K for $n^\star(\mathbf{k})$ in the superfluid at $T=1.6$ K. The $n^\star(\mathbf{k})$ calculated by Ceperley and Pollock (CP) are the same at $T=1.18$, 1.54, and 2.50 K, within statistical uncertainties. These $n^\star(\mathbf{k})$ are shown in the lower frame of Fig. 7. Also CP find $n_0\approx 7\pm 1\%$ at $T=1.18$ K, $n_0\approx 9\pm 1\%$ at $T=1.54$ K and $n_0\approx 0$ at $T=2.50$ K. If we renormalize all $n^\star(\mathbf{k})$ to the same n_0 value, say $n_0=0$, then all the calculated $n^\star(\mathbf{k})$ are the same, within statistical errors. Indeed, the calculated $n^\star(\mathbf{k})$ for $T=1.18$ K lies between $n^\star(\mathbf{k})$ for $T=1.54$ K and $T=2.5$ K. The $n(\mathbf{k})$ shown as the solid line in Fig. 7 is obtained from the data at $T=2.3$ K and is the same as the $n(\mathbf{k})$ calculated by CP at $T=2.50$ K. Thus, all evidence suggests that $n^\star(\mathbf{k})$ does not change from normal to superfluid ^{4}He. This follows physically, as noted above, because the zero-point energy (i.e., the kinetic energy per atom, approximately equal to 15 K), is much greater than the thermal energy at $T=2.3$ K. A further small reduction in T is unlikely to lead to significant redistribution within the $\mathbf{k}>0$ states.

We find a condensate fraction equal to $n_0=6\pm 2\%$ at $T=1.6$ K and SVP. This is based on the best-fit values of $n_0=5.0\pm 1.5\%$ in Fig. 2(a), the sensitivity to the

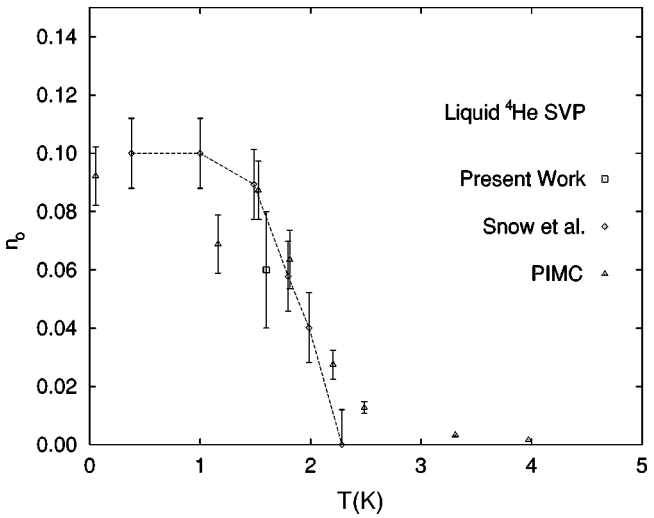

FIG. 8. Condensate fraction in liquid ^{4}He at SVP. Triangles are calculated (PIMC) values of Ceperley and Pollock (Ref. 24). The triangle at $T=0.1$ K is the calculated $T=0$ (GFMC) value of Whitlock and Panoff (Ref. 37). Diamonds are the observed values of Snow *et al.* (Ref. 32) with the dashed line as a guide to the eye. The square is the present value.

cutoff parameter k_c, which tends to increase n_0, and the nature of the fits near $y=0$. A very important conclusion is that n_0 cannot be zero. If n_0 is fixed at $n_0=0$, we obtain an $n(\mathbf{k})$ which differs dramatically from those observed experimentally at $T=2.3$ K and computed theoretically (PIMC) at all temperatures. We interpret this as evidence of a condensate in superfluid ^{4}He.

The present value of $n_0=6\pm2\%$ is compared to previously observed values and PIMC calculations in Fig. 8. We see that $n_0=6\pm2\%$ is somewhat lower than the observed value of Snow, Wang, and Sokol,[32] but well within the combined errors. The agreement with the PIMC value is good. From Fig. 6 we see that if we focused on the peak region ($y=0$) of the data only, then a higher value of n_0, around 8%, might be deduced. However, the fits in the wings of the distribution favor a lower value of n_0. The value of n_0 affects the wings through the FS broadening function $R(Q,y)$. For example, the observed $J(Q,y)$ may be written as a convolution of $n(\mathbf{k})$ and $R(Q,y)$ in the form

$$J(Q,y)=\int d\mathbf{k}n(\mathbf{k})R(\mathbf{Q},y-k_Q). \tag{19}$$

In Eq. (19), the condensate component $n_0\delta(\mathbf{k})$ of $n(\mathbf{k})$ leads to a term $n_0R(Q,y)$ in $J(Q,y)$. Thus, $J(Q,y)$ has a term proportional to $R(Q,y)$ with weight n_0 which contributes in the wings following $R(Q,y)$ as well as in the peak region. $R(Q,y)$ has oscillations in the wings but the data show no oscillations. A good fit in the wings and in the peak region leads to a lower value for n_0, to obtain uniform behavior. In previous measurements, more emphasis was placed on the agreement in the peak region of the data. This may account for the slightly lower n_0 value obtained here. Also, we have assumed here that the momentum distribution of the states above the condensate uncoupled from the condensate is the same in the superfluid as in the normal phase which may affect the value of n_0 obtained. Further measurements at low temperature are needed to establish whether there is indeed a significant difference.

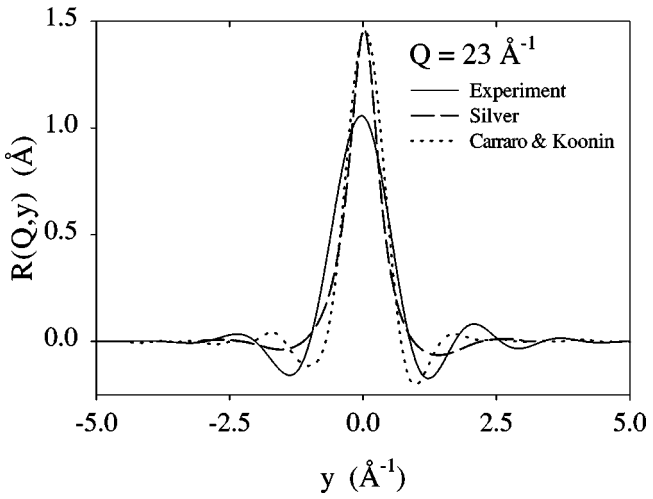

FIG. 9. Comparison of the extracted $R(Q,y)$ in liquid helium with theoretical calculations at $Q=23$ Å^{-1}.

Figure 3 shows that the FS function obtained here in the superfluid at $T=1.6$ K is the same as that obtained previously in normal ^{4}He at $T=2.3$ K. This is expected, since $R(Q,y)$ depends on the interactions in the fluid which change little with T. Precision measurements show that the pair-distribution function $g(r)$ changes little between superfluid and normal ^{4}He.[33,34] The $g(r)$ calculated here (see Fig. 10 and below) changes little between $T=1.6$ and 2.3 K. In a less accurate determination, we have also found[35] that $R(Q,y)$ is the same in liquid ^{3}He.

The present $R(Q,y)$ at $Q=23$ Å^{-1} is compared with the $R(Q,y)$ calculated by Silver and by Carraro and Koonin in Fig. 9. Both calculated $R(Q,y)$ are more sharply peaked than the $R(Q,y)$ observed here. The amplitude of the oscillations of $R(Q,y)$ at larger $|y|$ is smaller in the Silver function than observed here. Finally, the $R(Q,y)$ obtained here peaks at $y<0$ at all Q values, whereas both calculated functions appear to peak at $y>0$. Mazzanti *et al.*[40] have recently evaluated $R(Q,y)$ using the expression originally derived by Gersch and Rodriguez. In order to do this, they evaluated the two-body density matrix appearing in $R(Q,y)$. At $Q=23$ Å^{-1}, the peak height of their $R(Q,y)$ is similar to the calculated values shown in Fig. 9 and the oscillations are comparable to those in the $R(Q,y)$ by Carraro and Koonin and in the one observed here.

$R(Q,y)$ has been previously extracted from experiment by Sosnick *et al.*[14] and by Herwig *et al.*[36] Herwig *et al.* used the $n(\mathbf{k})$ and n_0 calculated by Whitlock and Panoff[37] at $T=0$ K in an expression similar to (19), and fitted the total $J(Q,y)$ to their data at $T=0.75$ K to obtain $R(Q,y)$. Their $R(Q,y)$ is generally narrower than the one obtained here, but broader than the calculated values, especially at lower Q values. At $Q=23$ Å^{-1} the peak height of their $R(Q,y)$ is the same as the calculated values shown in Fig. 9. Their observed $R(Q,y)$ always peaks at $y<0$.

The expansion used here to represent $R(Q,s)$ is exact up to powers s^6. The coefficients $\overline{\beta_n}$ are related to the moments of $R(Q,y)$. Since $R(Q,s)$ has no terms in s or s^2, the first and second moments of $R(Q,y)$ vanish. This is a well-

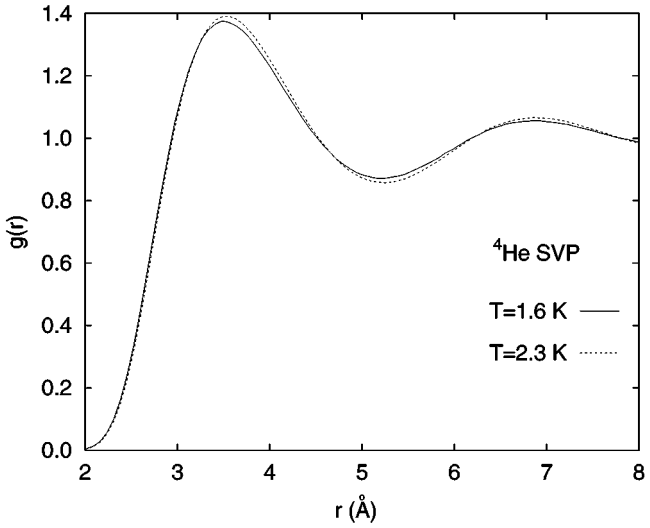

FIG. 10. Pair-distribution function $g(r)$ computed by PIMC in liquid helium at SVP, at $T=1.6$ K (solid line) and $T=2.3$ K (dashed line). Error bars are not shown for clarity; they are of the order of 0.02 or less.

known property of $R(Q,y)$. The observed $R(Q,y)$ peaks at $y<0$. This appears to be needed in order to get a positive third moment,

$$\int dy\ y^3 R(Q,y)=\overline{\beta_3}=\overline{a_3}/\lambda Q, \tag{20}$$

where

$$\overline{a_3}=\langle\nabla^2 V\rangle/6 \tag{21}$$

is positive. Both of the calculated $R(Q,y)$ shown in Fig. 9 peak at $y>0$ and may have a negative third moment. We return to a discussion of third and fourth moments below.

In order to obtain independent theoretical values of $\langle\nabla^2 V(r)\rangle$ and $\langle F^2=\mathbf{F}\cdot\mathbf{F}\rangle$, that appear in the third and fourth moments of $R(Q,y)$ respectively, as well as of the kinetic energy per particle $\langle E_K\rangle$, we carried out a path-integral Monte Carlo (PIMC) simulation of liquid helium at SVP, in the superfluid phase, at $T=1.6$ K, and in the normal phase at $T=2.3$ K. The PIMC method is a well-established tool that enables the computation of thermodynamic properties of quantum many-body systems at finite temperature directly from the microscopic Hamiltonian.[38] Here, we utilized it to calculate the kinetic energy per particle and the pair-distribution function $g(r)$. We carried out PIMC simulations of 108 helium atoms interacting via an accepted pairwise potential,[39] with periodic boundary conditions. This type of simulation has been shown to afford a quantitatively accurate microscopic description of condensed helium.[38] The pair-distribution function at the two temperatures investigated is shown in Fig. 10. From the pair-distribution function, we obtain $\langle\nabla^2 V(r)\rangle=32\pm4$ meV/Å^2 (30 ± 4 meV/Å^2) at $T=1.6$ K (2.3 K), and $\langle F^2\rangle=380\pm30$ (meV/Å)^2 (320 ± 30 (meV/Å)^2) at $T=1.6$ K (2.3 K). The computed values of the kinetic energy per particle and of the coefficients $\overline{a_3}$ and $\overline{a_4}$, obtained from $\overline{a_3}/\lambda=\langle\nabla^2 V(r)\rangle/6\lambda$ and $\overline{a_4}/\lambda^2=\langle F^2\rangle/3\lambda^2$ where $\lambda=\hbar^2/M=1.0443$ meV Å^2, are reported in Table I where they are compared to the values deduced from experiment. From Table I, we see that the calculated $\overline{a_3}$ values at the two temperatures lie above the observed values which are obtained from fits to the data. The difference is just outside the combined error. In the fit to the data, the magnitude of $\overline{a_3}$ is determined chiefly by the peak position of $J(Q,y)$, i.e., where $J(Q,y)$ falls on the ''energy'' transfer y scale. If there is a systematic error in determining the energy transfer in the measurement, this would translate into a systematic error in $\overline{a_3}$. We have checked the energy transfer by evaluating the first moment of the data and comparing it with the f-sum rule. We find that the scale and $\overline{a_3}$ are correct within the error quoted. In liquid Ne, the $\overline{a_3}$ determined from data in the same way agrees well with PIMC calculations.[42] Similarly, the calculated value of $\overline{a_4}$ lies above that obtained from a fit of $R(Q,s)$ to the data. We emphasize that $\overline{a_4}$ is actually very small and difficult to extract accurately from the fit. We believe that these discrepancies arise from the fitting of an $R(Q,s)$ which has a finite number of terms in the expansion to the data. The relatively few terms retained will attempt to simulate the full function if their number is insufficient to obtain convergence. For example, if only terms up to s^5 are retained, it is straightforward to show that the coefficient $\overline{a_4}$ would have to be negative in order to obtain an $R(Q,s)$ that converges at large s and reproduces experimental values. When terms up to s^6 are included in the expansion, the extracted $\overline{a_4}$ still lies below the expected value. This issue is discussed by Rinat *et al.*,[41] who have considered several fitting options. We emphasize that the difference between the calculated and extracted values of $\overline{a_3}$ and $\overline{a_4}$ are relatively small; in liquid neon, where $R(Q,y)$ is narrow compared to the momentum distribution, the extracted value of $\overline{a_3}$ agrees quantitatively with the PIMC-determined value, and $\overline{a_4}$ is positive.[42]

TABLE I. Comparison of the values of the kinetic energy per particle E_K (in K) and of the coefficients $\overline{a_3}/\lambda$ (in Å^{-4}) and $\overline{a_4}/\lambda^2$ (in Å^{-6}) computed by PIMC and deduced from experiment ($\lambda=\hbar^2/M=1.0443$ meV Å^2).

T	$\langle E_K\rangle$	$\overline{a_3}/\lambda$	$\overline{a_4}/\lambda^2$	Method
1.6	14.7 ± 0.1	5.1 ± 0.5	116 ± 10	PIMC
1.6	14.9 ± 0.35	2.8 ± 1.0	<50.0	Experiment
2.3	16.5 ± 0.1	4.8 ± 0.5	98 ± 10	PIMC
2.3	16.3 ± 0.35	3.3 ± 0.7	<50.0	Experiment

ACKNOWLEDGMENTS

This work was supported in part by the National Science Foundation through Research Grants INT-9314661, DMR-9623961, INT-9214242 and DMR 91234669. We acknowledge the financial support of the U. K. Engineering and Physical Science Research Council and the scientific support of the staff at the ISIS facility.

APPENDIX A

In this appendix we sketch the derivation of $n^\star(s)$ and $R(Q,s)$ leading to Eqs. (13) and (16), respectively. At high Q, the scattering time t and the distance $s=(\hbar Q/M)t$ traveled by the struck atom within the scattering time are short. This suggests a short-time expansion of $J(Q,s)$ and $J_{\rm IA}(s)$ in powers of s. Equations (3) and (5) are in the form natural for an expansion in cumulants. Expansion of Eq. (5) gives

$$J_{\rm IA}(s)=\exp\left[-\frac{\overline{\alpha_2}s^2}{2!}+\frac{\overline{\alpha_4}s^4}{4!}-\frac{\overline{\alpha_6}s^6}{6!}+\cdots\right], \quad \text{(A1)}$$

where

$$\overline{\alpha_2}=\langle k_Q^2\rangle, \quad \text{(A2)}$$

$$\overline{\alpha_4}=\langle k_Q^4\rangle-3\langle k_Q^2\rangle^2,$$

$$\overline{\alpha_6}=\langle k_Q^6\rangle-15\langle k_Q^4\rangle\langle k_Q^2\rangle+30\langle k_Q^2\rangle^3$$

are the cumulants of $n(k_Q)$. Since $n(k_Q)$ and $n(s)$ are even functions, Eq. (A1) has only even powers of s. A similar cumulant expansion of Eq. (3) yields[27]

$$J(Q,s)=\exp\left[-\frac{\overline{\mu_2}s^2}{2!}+\frac{i\overline{\mu_3}s^3}{3!}\cdots-\frac{\overline{\mu_6}s^6}{6!}+\cdots\right], \quad \text{(A3)}$$

where the $\overline{\mu_n}$ are similarly cumulants of the time-ordered $J(Q,s)$. The $\overline{\alpha_n}$ are clearly independent of Q. The $\overline{\mu_n}$ can be readily expressed as moments of $J(Q,y)$ and their Q dependence determined. An expansion of $R(Q,s)$ can be obtained directly from its definition $R(Q,s)=J(Q,s)/J_{\rm IA}(s)$ in Eq. (9) and the expansions (A1) and (A3) as

$$R(Q,s)=\exp\left[\frac{i\overline{\beta_3}s^3}{3!}+\frac{\overline{\beta_4}s^4}{4!}-\frac{i\overline{\beta_5}s^5}{5!}-\frac{\overline{\beta_6}s^6}{6!}+\cdots\right], \quad \text{(A4)}$$

where $\overline{\beta_n}=\overline{\mu_n}$ for odd n and $\overline{\beta_n}=\overline{\mu_n}-\overline{\alpha_n}$ for even n. From the moment expressions for the $\overline{\mu_n}$, the Q dependence of the $\overline{\beta_n}$ can be determined. Up to $n=6$ they are given by Eq. (17).

Equation (A1) describes only the short s behavior of $J_{\rm IA}(s)$ which arises from $n^\star(s)$. When there is a condensate, the OBDM $J_{\rm IA}(s)$ has long-range nearly constant components not described by the expansion (A1). These components must be added to the $J_{\rm IA}(s)$ given by Eqs. (A1) and (13) as discussed in Sec. II. Adding these components to $J_{\rm IA}(s)$ in Eq. (A1), we have, from Eqs. (13) and (15),

$$J_{\rm IA}(s)=n_0[1+f(s)]+A_1n^\star(s) \quad \text{(A5)}$$

and

$$J(Q,s)=\{n_0[1+f(s)]+A_1n^\star(s)\}R(Q,s), \quad \text{(A6)}$$

where this relation defines $R(Q,s)$ as in Eq. (9). The $n^\star(s)$ is again given by Eqs. (16) and (A1). Since $f(\mathbf{k})$ is sharply peaked near $\mathbf{k}=0$ similar to $\delta(\mathbf{k})$, $f(s)$ is long-ranged in s similar to the unit term in Eq. (A5). If $f(s)$ is approximated by a constant over the range of interest ($s\leqslant 5$ Å), then the only dependence on s in $n(s)$ appears in the $A_1n^\star(s)R(Q,s)$ term. Physically, we know that $J(Q,s)$ vanishes at large s even though $n(s)$ has long-range components. Using the cumulant expansion (A3) again for $J(Q,s)$ in Eq. (A6), shows that $R(Q,s)$ must again have a series representation as in Eq. (A4). Assuming that $(n_0[1+f(s)]$ is constant independent of s we can show that the coefficients in the expansion of $R(Q,s)$ are again given exactly by Eq. (17). Thus Eqs. (16) and (17) hold in the superfluid as well as in normal ^{4}He. The central assumption underlying this representation of $R(Q,s)$ is that $n_0[1+f(s)]$ is constant over the range of $R(Q,s)$, i.e., between $s=0$ and the value of s at which $R(Q,s)$ goes to zero.

APPENDIX B

In this appendix we discuss the fitting procedure and the errors in the fitted parameters. The values of the parameters n_0 and the $\overline{\beta_n}$ in $J(Q,y)$ at each Q were determined by fitting $J(Q,y)$ given by Eq. (10), properly convoluted with the instrument resolution, to the data. The best fit $J(Q,y)$ and hence the best values of the parameters were found by minimizing the mean-square deviation χ^2 of the convoluted $J(Q,y)=j_i$, from the data, d_i, using the standard definition

$$\chi^2=\frac{1}{N-M+1}\sum_{i=1}^{N}\left(\frac{d_i-j_i}{\sigma_i}\right)^2. \quad \text{(B1)}$$

Here N is the number of data points at each Q (typically 120), M is the number of adjustable parameters (typically 4) and σ_i is the error in the data. The error bars on the parameters were calculated by the fitting program (the ISIS Frills package) assuming a linear relation between the calculated function and the parameters. Typical fits are shown in Fig. 1 and the resulting parameters and their errors at each Q are shown in Fig. 2. The magnitude of the error reflects the statistical error of the data at a given Q and the sensitivity of the fit to that parameter. A small error bar implies a high sensitivity.

With N large, as the case here, χ^2 should take values of $0.8<\chi^2<1.2$, approximately. A small χ^2 suggests that the error σ_i in the data is overestimated. A large χ^2 signals a poor fit. The best fit at $Q=29$ Å^{-1} shown in Fig. 1, with n_0, $\overline{\beta_3}$, $\overline{\beta_5}$, and $\overline{\beta_6}$, adjusted (which yielded $n_0=0.057$) has a $\chi^2=0.956$. With n_0 arbitrary fixed at $n_0=0.07$, and the $\overline{\beta_n}$ refined to obtained a best fit, we find a $\chi^2=1.06$. Thus the values of χ^2 are reasonable and the quality of the fit is quite sensitive to n_0. In contrast, the fit at $Q=29$ Å^{-1} shown in the upper frame of Fig. 7, in which n_0 is fixed at $n_0=0$, $R(Q,y)$ was set to the normal-liquid ^{4}He value shown in Fig. 3, and the parameters $\overline{\alpha_n}$ in $n(\mathbf{k})$ adjusted to get a best fit, has a $\chi^2=1.40$. This suggests a significantly poorer fit.

Particularly to be noted in Fig. 2 is that the fluctuation of the $\overline{\beta_6}$ values from Q to Q is significantly greater than the error bar on $\overline{\beta_6}$ calculated by the fitting program at a given Q. The data was normalized separately at each Q. Additional statistical error from Q to Q can arise from this separate normalization. We believe that the fluctuation of the parameters from Q to Q best represents the total statistical error in the parameters. The error in the quoted average value of

$\overline{\beta_6}Q^2 = 175 \pm 75$ Å^{-8} was set so that the mean value plus errors cover 68% of the 29 separate determinations of $\overline{\beta_6}Q^2$.

We also made an independent check on the uncertainty in the determination of $\overline{\beta_6}$ and n_0 at a given Q by varying these parameters and noting the change in χ^2. Given the definition of χ^2 above and assuming that the N is large enough that the χ^2 have a Gaussian distribution about the least value $\chi^2 \sim 1$, a change of $\overline{\beta_6}$ by one standard deviation should change χ^2 by approximately $1/\sqrt{N}$. At $Q = 29$ Å^{-1} we found that χ^2 was increased from its least value of 0.956 obtained for $\overline{\beta_6}Q^2 = 280$ to 1.05 for $\overline{\beta_6}Q^2 = 160$ and 445 Å^{-1} suggesting that $\overline{\beta_6}Q^2 = 280 \pm 140$ Å^{-8}. This error is greater than the error calculated by the fitting program and is consistent with the final error in $\overline{\beta_6}Q^2$ obtained from fluctuations from Q to Q. Similarly, we found $\chi^2 = 1.05$ for $n_0 = 0.069$ and 0.045 suggesting that $n_0 = 0.057 \pm 0.12$ emerges from the fit. This is also consistent with the error of ± 0.015 assigned to n_0 due to its variation from Q to Q.

*Current address: Hahn-Meitner-Institut, Glienicker Strasse 100, 14109 Berlin, Germany.

†Current address: Oliver Lodge Laboratory of Physics, University of Liverpool, Oxford Street, Liverpool L69 3BX, UK.

‡Current address: Department of Physics, San Diego State University, San Diego, California 92182.

[1] S. N. Bose, Z. Phys. **26**, 178 (1924).

[2] A. Einstein, Sitzungsber. K. Preuss. Akad. Wiss., Phys. Math. K1. **1924**, 261 (1924).

[3] F. London, Nature (London) **141**, 643 (1938); Phys. Rev. **54**, 947 (1938).

[4] *Bose-Einstein Condensation*, edited by A. Griffin, D. W. Snoke, and S. Stringari (Cambridge University Press, Cambridge, 1995).

[5] M. H. Anderson *et al.*, Science **269**, 198 (1995).

[6] K. B. Davis *et al.*, Phys. Rev. Lett. **75**, 3969 (1995).

[7] P. Nozières and D. Pines, *Theory of Quantum Liquids* (Addison-Wesley, Reading, MA, 1990).

[8] A. Griffin, *Excitations in a Bose-Condensed Liquid* (Cambridge University Press, Cambridge, 1993).

[9] H. R. Glyde, *Excitations in Liquid and Solid Helium* (Oxford University Press, Oxford, 1994).

[10] V. F. Sears, E. C. Svensson, P. Martel, and A. D. B. Woods, Phys. Rev. Lett. **49**, 279 (1982).

[11] E. C. Svensson and V. F. Sears, in *Frontiers of Neutron Scattering*, edited by R. J. Birgeneau, D. E. Moncton, and A. Zilinger (North-Holland, Amsterdam, 1986).

[12] T. R. Sosnick, W. M. Snow, P. E. Sokol, and R. N. Silver, Europhys. Lett. **9**, 707 (1989).

[13] T. R. Sosnick, W. M. Snow, and P. E. Sokol, Phys. Rev. B **41**, 11 185 (1990).

[14] T. R. Sosnick, W. M. Snow, R. N. Silver, and P. E. Sokol, Phys. Rev. B **43**, 216 (1991).

[15] P. E. Sokol and W. M. Snow, in *Excitations in Two-Dimensional and Three-Dimensional Quantum Fluids*, NATO ASI Series B, Vol. 257, edited by A. F. G. Wyatt and H. J. Lauter (Plenum, New York, 1991).

[16] P. E. Sokol, in *Bose-Einstein Condensation*, edited by A. Griffin, D. W. Snoke, and S. Stringari (Cambridge University Press, Cambridge, 1995).

[17] A. Miller, D. Pines, and P. Nozières, Phys. Rev. **127**, 1452 (1962).

[18] P. C. Hohenberg and P. M. Platzman, Phys. Rev. **152**, 198 (1966).

[19] P. Martel, E. C. Svensson, A. D. B. Woods, V. F. Sears, and R. A. Cowley, J. Low Temp. Phys. **23**, 285 (1976).

[20] H. A. Gersch and L. J. Rodriguez, Phys. Rev. A **8**, 905 (1973).

[21] V. F. Sears, Phys. Rev. B **30**, 44 (1984), and references therein.

[22] R. T. Azuah, W. G. Stirling, H. R. Glyde, P. E. Sokol, and S. M. Bennington, Phys. Rev. B **51**, 605 (1995).

[23] R. N. Silver, Phys. Rev. B **37**, 3794 (1988).

[24] D. M. Ceperley and E. L. Pollock, Can. J. Phys. **65**, 1416 (1987).

[25] R. N. Silver, Phys. Rev. B **39**, 4022 (1989).

[26] C. Carraro and S. E. Koonin, Phys. Rev. Lett. **65**, 2792 (1990).

[27] H. R. Glyde, Phys. Rev. B **50**, 6726 (1994).

[28] J. Gavoret and P. Nozières, Ann. Phys. (N.Y.) **28**, 349 (1964).

[29] K. H. Andersen, W. G. Stirling, R. Scherm, A. Stunault, B. Fåk, A. Godfrin, and A. J. Dianoux, J. Phys. C **6**, 821 (1994).

[30] C. K. Loong, S. Ikeda, and J. M. Carpenter, Nucl. Instrum. Methods Phys. Res. A **260**, 381 (1987).

[31] S. Ikeda and J. M. Carpenter, Nucl. Instrum. Methods Phys. Res. A **239**, 536 (1985).

[32] W. M. Snow, Y. Wang, and P. E. Sokol, Europhys. Lett. **19**, 403 (1992).

[33] E. C. Svensson, V. F. Sears, A. D. B. Woods, and P. Martel, Phys. Rev. B **21**, 3638 (1980).

[34] V. F. Sears and E. C. Svensson, Int. J. Quantum Chem., Quantum Chem. Symp. **14**, 715 (1980).

[35] R. T. Azuah *et al.*, Physica B **213-214**, 454 (1995).

[36] K. W. Herwig, P. E. Sokol, W. M. Snow, and R. C. Blasdell, Phys. Rev. B **44**, 308 (1991).

[37] P. A. Whitlock and R. M. Panoff, Can. J. Phys. **65**, 1409 (1987).

[38] For a thorough description of the PIMC methodology, see D. M. Ceperley, Rev. Mod. Phys. **67**, 279 (1995).

[39] R. A. Aziz, M. J. Slaman, A. Koide, A. R. Allnatt, and W. J. Meath, Mol. Phys. **77**, 321 (1992).

[40] F. Mazzanti, J. Boronat, and A. Polls, Phys. Rev. B **53**, 5661 (1996).

[41] A. S. Rinat, M. F. Taragin, F. Mazzanti, and A. Polls (unpublished).

[42] R. T. Azuah, W. G. Stirling, H. R. Glyde, and M. Boninsegni, J. Low Temp. Phys. **109**, 287 (1997).